JOURNAL OF NEUROPHYSIOLOGY
Vol. 74, No. 3, September 1995. *Printed in U.S.A.*

Intracellular Ca^{2+} Stores Can Account for the Time Course of LTP Induction: A Model of Ca^{2+} Dynamics in Dendritic Spines

A. SCHIEGG, W. GERSTNER, R. RITZ, AND J. LEO VAN HEMMEN
Institute of Theoretical Physics, Physik-Department der TU München, D-85748 Garching bei München, Germany

SUMMARY AND CONCLUSIONS

1. A model of Ca^{2+} dynamics in spines of CA1 hippocampal neurons is presented. In contrast to traditional models, which concentrate on the effects of Ca^{2+} influx, diffusion, buffering, and extrusion, we also consider the additional effect of intracellular Ca^{2+} stores.

2. It is shown that traditional models without Ca^{2+} stores cannot account for the time course of long-term potentiation (LTP) induction as found in recent experiments. Experimental data suggest that the intracellular Ca^{2+} concentration should be elevated for up to 2 s, whereas the Ca^{2+} concentration in standard models of Ca^{2+} dynamics decays much faster.

3. When intracellular Ca^{2+} stores are taken into account, a much slower decay is found. In particular, a model simulation with a stimulation paradigm consisting of two bursts of four impulses at 100 Hz each and variable interburst intervals can reproduce experimental results found for primed or theta-burst stimulation.

4. In our model, Ca^{2+} release from the store has a nonlinear, bell-shaped dependence on the intracellular Ca^{2+} concentration, similar to the one found for inositoltrisphosphate and ryanodine receptors. These receptors are known to control calcium release from intracellular stores.

5. Our model suggests an important role of intracellular calcium stores in the induction of LTP. The stores serve as a long-term calcium source that can sustain an intracellular Ca^{2+} concentration above the resting level for 1–2 s.

INTRODUCTION

Long-term potentiation (LTP) of synaptic efficacy has been extensively studied during recent years, both in experiments (for reviews, see for example Bindman et al. 1991; Brown et al. 1991; Madison et al. 1991) and in model approaches (Brown et al. 1988; Gamble and Koch 1987; Gold and Bear 1994; Holmes and Levy 1990; Kitajima and Hara 1990; Zador et al. 1990). This interest is partly due to the fact that LTP could be the neuronal implementation of a Hebbian learning rule (Hebb 1949) that is used, in one form or another, in various mathematical models of neural networks (cf. for example Amit 1989; Domany et al. 1991; Hertz et al. 1991; Müller and Reinhard 1991; Peretto 1992). Phenomenologically, LTP of a synaptic link between presynaptic and postsynaptic neurons, e.g., in the CA1 region of the hippocampus, can be induced if brief tetanic stimuli to presynaptic pathways are applied. The exact molecular mechanism leading to the potentiation is still unclear (Brown et al. 1991; Lisman and Harris 1993; Madison et al. 1991). It has, however, been shown in several experiments that a transient rise of the intracellular Ca^{2+} concentration ($[Ca^{2+}]$) is a necessary condition for LTP induction (Bliss and Collingridge 1993). To explain this, calcium influx through *N*-methyl-D-aspartate (NMDA) receptor channels has been assumed to be the essential source of calcium. Models of Ca^{2+} dynamics in which NMDA channels are the only source of calcium yield a time course of intracellular $[Ca^{2+}]$ that is consistent with experimental findings on CA1 hippocampal neurons, at least for the tetanic stimulus paradigm (Gamble and Koch 1987; Gold and Bear 1994; Holmes and Levy 1990; Zador et al. 1990). There is, however, a key experiment by Malenka et al. (1992) that makes a reconsideration of Ca^{2+} dynamics during LTP induction inevitable. In this experiment a weak stimulation scenario of 100 impulses at 100 Hz was used. Under normal conditions, this stimulation paradigm leads to reliable induction of LTP. By activation of a photolabile Ca^{2+} buffer, however, it was possible to limit the rise in intracellular Ca^{2+} to a specified period. It turned out that LTP was induced only if the Ca^{2+} buffer was activated $>2-2.5$ s after the beginning of the stimulus. In the following, we will refer to this as the 2-s criterion. It is safe to conclude from this experiment that the intracellular $[Ca^{2+}]$ has to be elevated for ≥ 1.5 s after the stimulus to successfully induce LTP. Our simulation studies, presented below, will show that this cannot be achieved if NMDA channels or other voltage-gated Ca^{2+} channels are the only source of calcium.

To account for the 2-s criterion, we propose an extended model that takes intracellular Ca^{2+} stores into account. Over the past two or three years there has been growing evidence for an important role of intracellular Ca^{2+} stores in the induction of LTP. Ca^{2+} release from these stores is mediated by ryanodine receptors (RYR) and inositol 1,4,5-trisphosphate ($InsP_3$) receptors, as has been shown in a variety of experiments. Drugs that deplete intracellular calcium stores (thapsigargin) or inhibit calcium-induced calcium release from intracellular stores (ryanodine) substantially reduce the transient rise in intracellular $[Ca^{2+}]$ during synaptic activation of NMDA channels (Bliss and Collingridge 1993). On the other hand, the induction of LTP is inhibited by applying thapsigargin and dantrolene, a drug that blocks the ryanodine receptor (Harvey and Collingridge 1992; Obenaus et al. 1989). Activation of metabotropic glutamate receptors, which play a role during $InsP_3$ synthesis, can induce LTP without the participation of NMDA receptors (Bortolotto and Collingridge 1993). Because this mechanism is sensitive to thapsigargin, it is most likely that release of Ca^{2+} from intracellular stores alone can be sufficient for the induction of LTP. These experiments imply an important role of intracellular stores in the induction of LTP.

0022-3077/95 $3.00 Copyright © 1995 The American Physiological Society

The simulations of Gamble and Koch (1987), Zador et al. (1990), and Holmes and Levy (1990) using NMDA channels as the principal source of Ca^{2+} during LTP induction have shown that the amplitude of a transient rise in the intracellular $[Ca^{2+}]$ is directly related to both the stimulation frequency and the number of coactivated synapses. Because in experiments there is a similar relation between LTP and the stimulation frequency or the number of stimulated synapses (Madison et al. 1991), it is likely that there is a direct connection between the maximum intracellular $[Ca^{2+}]$ and the induction of LTP. In this interpretation the models give a qualitative, if not quantitative, explanation of the experiments. On the other hand, the above models cannot account for the experimental results of Malenka et al. (1992). In fact, our model studies presented in this paper show that the $[Ca^{2+}]$ decays too fast after the end of the stimulus to account for the 2-s criterion, if NMDA receptors were the only Ca^{2+} source (*Simulations of the experiment of Malenka et al. with standard dynamics,* below). In our opinion, intracellular stores serving as "long-term" calcium sources could bridge the gap between the short-time and the long-time behavior. Here we present an extended model including intracellular Ca^{2+} stores. The model is introduced in METHODS. It is applied to the experiments of Malenka et al. (1992) in *Simulations of the experiment of Malenka et al. with intracellular stores.* Furthermore, it is shown that the extended model can also explain the time course of the induction of LTP with primed and theta-burst stimulation (*Intracellular stores with primed and theta-burst stimulation*). These stimulation patterns are of particular interest because they resemble activity patterns measured in vivo in hippocampus. We close with a discussion of our results.

METHODS

In our simulations we use a nine-compartment electrical model of a CA1 pyramidal cell (Fig. 1) to which an equivalent circuit of a synapse (Fig. 2) has been attached. In the first part of our simulations (*Simulations of the experiment of Malenka et al. with standard dynamics*), calcium dynamics in the dendritic spine have been modeled on the basis of the approach of Zador et al. (1990). Spine head and spine neck are assumed to be cylindrical and consist of several diffusion compartments. Ca^{2+} that enters the spine head through NMDA channels diffuses into the spine neck and the dendrite, is buffered by intracellular buffers, and is pumped out of the spine by calcium extrusion mechanisms. The central results in *Simulations of the experiment of Malenka et al. with intracellular stores* and *Intracellular stores with primed and theta-burst stimulation* have been achieved with an extended model that also includes intracellular calcium stores in the spine head. The description of calcium stores is given in *Model of intracellular calcium stores,* whereas the basic model is introduced in *Equivalent circuit for a synapse, Model neuron,* and *Standard calcium dynamics.*

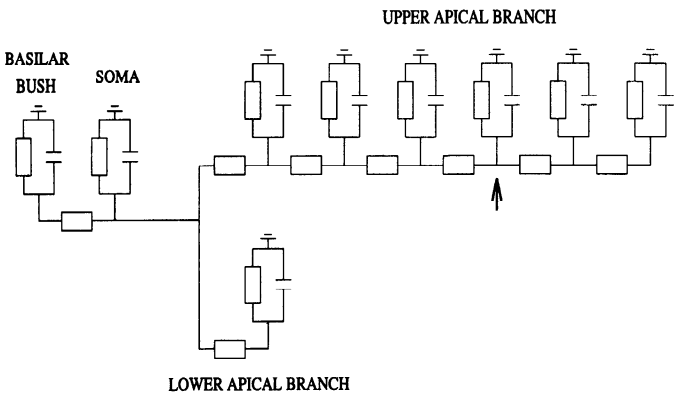

FIG. 1. Model neuron with 9 compartments. To allow a good spatial resolution in the neighborhood of the synaptic input (arrow), the upper apical branch has been divided into 6 compartments. The other branches are reduced to a single compartment only. The following parameters were used: membrane resistance, basilar compartment: R = 240 MΩ; lower apical compartment: R = 240 MΩ; soma: R = 3,000 MΩ; and for each upper apical compartment: R = 1800 MΩ. Core resistances: r = 18 MΩ for the upper apical compartments and r = 60 MΩ for the lower apical branch and the basilar bush. The capacitances were computed from $C = R/\tau$ with τ = 30 ms. The batteries for leak voltage are not shown. The arrow refers to the synapse of Fig. 2.

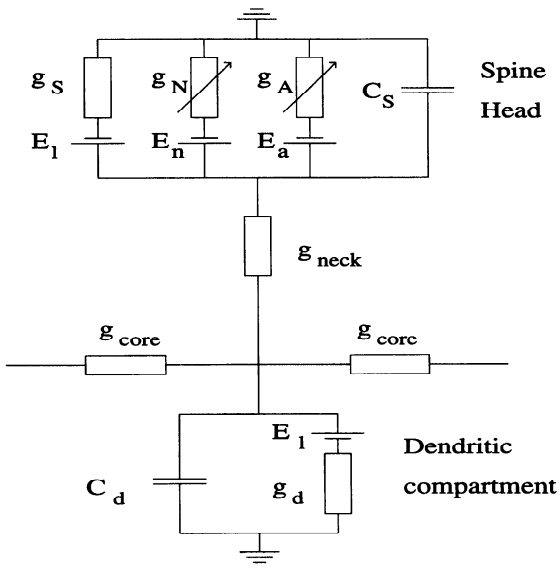

FIG. 2. Electrical model of a synapse on an spine. The conductivities g_N and g_A for the *N*-methyl-D-aspartate (NMDA) and α-amino-3-hydroxy-5-methyl-4-isoxazolepropionic acid (AMPA) channels, respectively, are described by time-dependent functions; see the text for details. The spine capacitance C_s and the conductivity g_s of the spine membrane, and the spine neck conductivity g_{neck} are constant parameters (C_s = 0.04 pF, $g_s = \tau/C_s$, E_l = −80 mV, g_{neck} = 1/100 MΩ, and $E_n = E_a = 0$) where E_l, E_n, and E_a are the reversal potentials of leakage, NMDA, and AMPA channels, respectively. C_d is the capacitance, g_d and g_{core} are the transversal and longitudinal conductivity of a dendritic compartment.

Equivalent circuit for a synapse

The passive electrical properties of the spine head membrane are modeled by a capacitor C_s parallel to a leak conductance g_s. A battery E_l in series with g_s provides the resting potential of the membrane. We consider two types of neurotransmitter-gated ion channels, α-amino-3-hydroxy-5-methyl-4-isoxazolepropionic acid (AMPA) and NMDA channels, both described as time-dependent conductivities, g_A and g_N, respectively. The spine head is connected to the dendrite through the spine neck, which is described by a static conductivity, g_{neck} (Fig. 2).

As in earlier studies (Gamble and Koch 1987; Zador et al. 1990), the time-dependent conductivity of the AMPA channel is described by an α-function. More precisely, the AMPA current in response to a single presynaptic spike at t = 0 is

$$I_{ampa}(t) = (V - E_a)\,\frac{e}{t_p}\,g_p t \exp\left(\frac{-t}{t_p}\right) \qquad (1)$$

where V is the spine head potential, E_a is the AMPA reversal potential, g_p is the maximum AMPA conductivity, e is the Euler

TABLE 1. *Electrical parameters*

Description	Parameter	Value
AMPA channels		
Reversal potential	E_a	0V
Maximum conductance	g_p	0.5 nS
Channel time constant	t_p	1.5 ms
NMDA channels		
Reversal potential	E_n	0V
Maximum conductance	g_n	0.2 nS
Channel closing time	τ_1	80 ms
Channel opening time	τ_2	0.67 ms
Prefactor of magnesium block	η	0.33/mM
Voltage factor of magnesium block	γ	0.06/mV
Magnesium concentration	$[Mg^{2+}]$	1.2 mM
Global electrical constants		
Membrane time constant	τ	30 ms
Specific membrane resistance	R_m	30 kΩ/cm^2
Specific membrane capacity	C_m	1 μF/cm^2
Input resistance	R_{in}	100 MΩ
Compartment constants		
Resistance, somatic compartment	R_{soma}	3,000 MΩ
Resistance, dendritic compartments	$(g_d)^{-1}$	1,800 MΩ
Resistance, basilar bush	R_{bb}	240 MΩ
Resistance, lower apical branch	R_{la}	240 MΩ
Resistance, spine head	$(g_s)^{-1}$	750 GΩ
Longitudinal conductance, dendritic compartment	g_{core}	(18 MΩ)$^{-1}$
Longitudinal conductance, basilar bush	g_{bb}	(60 MΩ)$^{-1}$
Longitudinal conductance, lower apical branch	g_{la}	(60 MΩ)$^{-1}$
Longitudinal conductance, spine neck	g_{neck}	(100 MΩ)$^{-1}$

AMPA, α-amino-3-hydroxy-5-methyl-4-isoxazolepropionic acid; NMDA, *N*-methyl-D-aspartate.

constant, and $t > 0$ is the time after the stimulation. For the NMDA current we use a double exponential (Zador et al. 1990)

$$I_{nmda} = (V - E_n) g_n \frac{\exp(-t/\tau_1) - \exp(-t/\tau_2)}{1 + \eta \cdot [Mg^{2+}] \cdot \exp(-\gamma V)} \qquad (2)$$

where E_n is the NMDA reversal potential and g_n is a conductivity parameter. Depending on the membrane voltage, NMDA channels are blocked by Mg^{2+} ions. This is expressed by the denominator in the above equation, whereas the numerator expresses the intrinsic conductivity of the NMDA channels. Constants in *Eq. 2* are adjusted according to measurements as discussed in Zador et al. (1990) and Brown et al. (1991). We adopt the parameters of Zador et al. (1990) listed in Table 1.

LTP induction involves the coactivation of many synapses. For the sake of simplicity, we did not model tens or hundreds of synapses explicitly. Instead we made two assumptions.

1) All coactivated synapses are situated in a relatively small area of the neuron.

2) These synapses are activated synchronously.

Because of the first assumption, we can attach all coactivated synapses to the same dendritic compartment. Let us consider the synaptic input current I_{syn} into a specific spine head with index i that is attached to the dendritic compartment under consideration. The change of spine head voltage $V_{s,i}$ is described by

$$\frac{dV_{s,i}}{dt} = \frac{1}{C_s} [g_s(E_l - V_{s,i}) + g_{neck}(V_d - V_{s,i}) + I^{syn}] \qquad (3)$$

The dendritic compartment is coupled to N of these synapses, yielding

$$\frac{dV_d}{dt} = \frac{1}{C_d} [g_d(E_l - V_d) - \sum_{i=1}^{N} g_{neck}(V_d - V_{s,i}) + I^{long}] \qquad (4)$$

where V_d is the membrane voltage in the dendritic compartment. The capacitance C_d and the conductivity g_d are dendritic membrane parameters and I_{long} denotes longitudinal currents from other dendritic compartments. If all synapses are activated synchronously and if they are all connected to the same dendritic compartment, then the time course $V_{s,i}(t)$ is identical for all spine heads $1 \le i \le N$. In this case, we can replace the sum over N by a multiplication with the factor N

$$\frac{dV_d}{dt} = \frac{1}{C_d} [g_d(E_l - V_d) - N g_{neck}(V_d - V_{s,i}) + I^{long}] \qquad (5)$$

In real neurons, synchronous coactivation of many synapses is rather unlikely. Also, coactivated synapses will in general not be located on the same dendritic compartment. Because, according to *Eq. 1* and *2*, the input current is a function of the local membrane potential, summation of different inputs is nonlinear and, in general, depends on the location of all coactivated synapses. For these reasons, we consider the factor N in our simplified approach (*Eq. 5*) not as an exact measure of the number of coactivated synapses but rather as a semiquantitative measure of the overall stimulation strength.

Model neuron

We model a pyramidal cell with two major apical dendrites and a basilar bush as commonly found in the hippocampal CA1 region (e.g., Turner and Schwartzkroin 1980) by a simplified neuron model with nine compartments (Fig. 1). The stimulated synapses are assumed to be located on the fourth compartment of the upper branch of the apical dendrite. This branch has been divided in six equal compartments to model a smooth spread of the incoming signals. Soma, lower apical branch, and basilar bush are modeled by a single compartment only. We have checked by preliminary simulations with more complex model neurons that the above nine compartments are sufficient for an accurate description of the electrical potential in the model spine head on the upper apical dendrite; and this is where we will focus.

For the electrical constants of the neuron, we use typical values listed in Table 1. The values for $\tau = 30$ ms and input resistance (R_{in}) = 100 MΩ have been taken from the paper of Spruston and Johnston (1992), the values for specific membrane capacity (C_m) from Brown et al. (1981), and the membrane resistance has been computed from specific membrane resistance (R_m) = τ/C_m. The electrotonic length (L) is assumed to be 0.7 for each of the apical branches and the basilar bush. We assume a soma membrane surface of 1,000 μm^2 corresponding to a soma membrane resistance of 3,000 MΩ. The input conductivities of the dendritic branches have been computed by standard procedures (Perkel and Mulloney 1978) from R_{in} and L. In particular, for the core and membrane resistance of the six compartments of the the upper apical dendrite, we find values of 18 and 1 800 MΩ, respectively. It turns out that our results are not sensitive to the precise value of these parameters. Thus the values have been fixed in some plausible regime. The computer code has been developed locally. The system of differential equations has been integrated numerically with the program lsoda of the odepack library (Hindmarsh 1983; Petzold 1983). This is a standard library routine for stiff and nonstiff equations. The program adjusts the integration step automatically during each run. In our simulations, numerical values were written in a file after every 0.1 ms of simulated time. This limits the integration step to a maximum size of 0.1 ms. If necessary, shorter steps where

chosen automatically on the basis of the criterion that the estimated error stays below a value of 0.1 nV for each voltage variable and below a value of 0.1 nM for concentration variables.

To test our model, we have simulated the activation of one or several synapses in the upper apical dendrite, cf. Fig. 3, *A* and *B*. The depolarization of the spine head due to a single spike at a single synapse (Fig. 3*B*, *inset*) is in the range of several millivolts, as in other models with up to several thousand dendritic compartments (Brown et al. 1991; Holmes and Levy 1990). Figure 3*A*, *inset*, shows the somatic excitatory postsynaptic potential (EPSP) caused by the activation of a single synapse. It has been estimated elsewhere that the activation of a single synapse causes a somatic EPSP with an amplitude of several hundred microvolts (McNaughton et al. 1981). Our result is in the expected range. Note that a spike train of four spikes at 100 Hz leads to a pronounced summation at the soma, but there is only a small increase of the peak voltage at the spine head. If 30 synapses are coactivated simultaneously (Fig. 3, *A* and *B*, full-sized graphs), there is a strong depolarization both at the spine head and the soma.

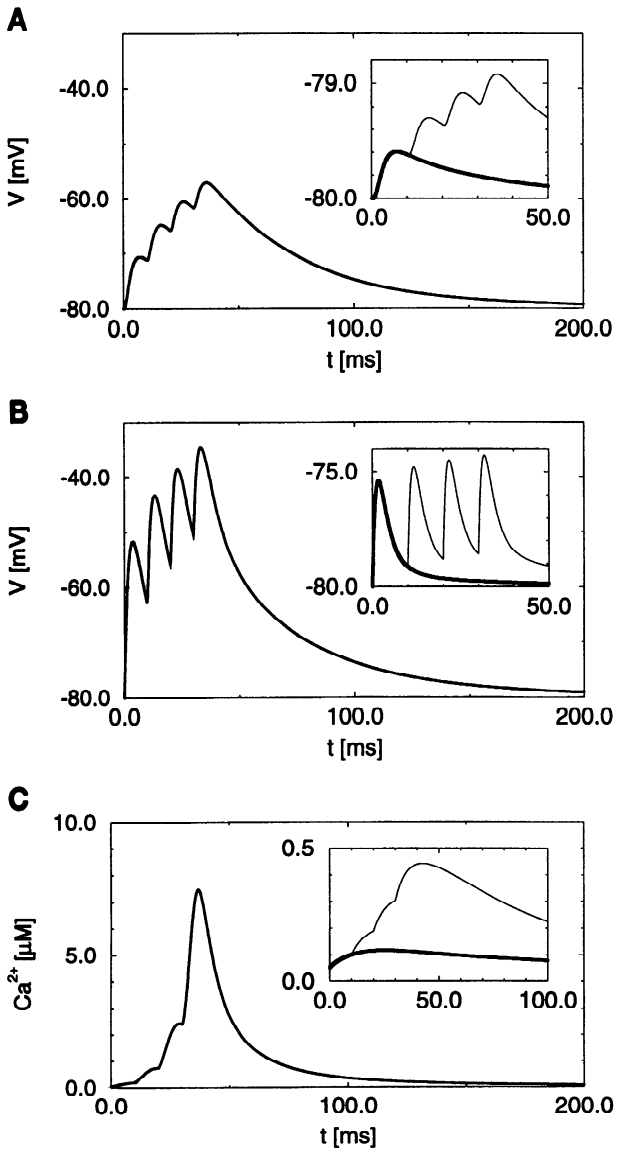

FIG. 3. Response to synaptic input. *A*: simulated postsynaptic potential at the soma. *B*: voltage at the spine head. *C*: calcium concentration in the spine head. In the simulations plotted in the full-sized graphs, the neuron has been activated at $N = 30$ synapses with a burst of 4 spikes at 100 Hz. *Insets*: respective quantities after 1 (thick lines) or 4 (thin lines) spikes at a single synapse. A single spike evokes a depolarization of ~0.4 mV at the soma (*A*) and ~5 mV at the spine head (*B*). Subsequent spikes lead to a summation effect, which is most pronouncedly seen at the soma. Note the different scales *insets* of *A* and *B*. The calcium amplitude (*C*) in response to a single spike is ~0.1 μM. More spikes or a larger number of coactivated synapses lead to a higher calcium concentration in the spine head.

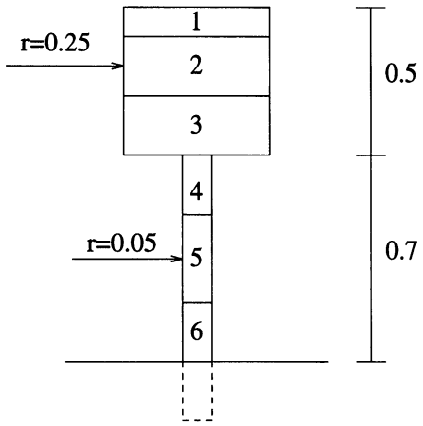

FIG. 4. Model of Ca^{2+} dynamics in a dendritic spine. To describe calcium diffusion, the spine has been discretized into 6 diffusion compartments labeled 1–6. The length scale indicated by the bar at *right* is given in μm. In our simulations, the dendrite below compartment 6 contains a constant calcium concentration of 0.5 μM.

Standard calcium dynamics

Our model of standard calcium dynamics follows Zador et al. (1990). It includes Ca^{2+} pumps to extrude calcium from the cell in addition to Ca^{2+} buffers, NMDA channels, and calcium diffusion.

Spine head and spine neck are assumed to be cylindrical. For Ca^{2+} diffusion, we use a discretized form of the diffusion equation

$$\frac{\partial[Ca^{2+}]}{\partial t} = D\left\{\frac{\partial^2}{\partial x^2} + \frac{\partial^2}{\partial y^2} + \frac{\partial^2}{\partial z^2}\right\}[Ca^{2+}] \qquad (6)$$

where x, y, and z are spatial coordinates and $D = 0.6\ \mu m^2/s$ is the diffusion coefficient of calcium. Spine head and spine neck consist of three diffusion compartments each (see Fig. 4). Radial diffusion was neglected. This has been checked using several more accurate discretizations with and without radial diffusion, without any significant difference of the results.

Ca^{2+} enters the spine head at the top of the spine through NMDA channels. The Ca^{2+} current is assumed to be a fixed fraction of 10% of the total NMDA current ($I_{Ca2+} = 0.1 \times I_{NMDA}$) (Garaschuk 1995).

It is known that there are large intracellular quantities of calmodulin (CaM) and smaller unknown quantities of other Ca^{2+} binding proteins. We have included CaM as a Ca^{2+} buffer in our model. CaM has four Ca^{2+} binding sites per molecule, to which Ca^{2+} is bound sequentially (Klee et al. 1980). The intracellular CaM concentration is estimated to lie at ~30 μM (Carafoli 1987). Thus we have chosen a concentration of Ca^{2+} binding sites of $[bu_{tot}]_i = 120\ \mu M$ for all compartments $1 \le i \le 6$. Cooperativity effects due to sequential binding at the four different sites have been neglected. To check this assumption, we included sequential binding in some simulations and we sometimes also doubled the CaM concentration in the first compartment (which may be considered as the locus of the postsynaptic density), but this did not modify the results. A standard rate equation for binding of Ca^{2+} to buffer molecules yields for the change of the free calcium concentration in compartment i due to buffering

$$\frac{d[Ca^{2+}]_i}{dt} = -k_f[Ca^{2+}]_i[bu_{free}]_i + k_r([bu_{tot}]_i - [bu_{free}]_i) \qquad (7)$$

while at the same time the concentration of free buffering site $[bu_{free}]_i$ changes according to

$$\frac{d[bu_{free}]_i}{dt} = -k_f[Ca^{2+}]_i[bu_{free}]_i + k_r([bu_{tot}]_i - [bu_{free}]_i) \quad (8)$$

Here, $[bu_{tot}]_i$ is the total concentration of buffering sites in compartment i, whereas k_f and k_r are the forward and backward buffering rates, respectively. The buffering rates are unknown but there are estimates for the dissociation constant $K_d \approx 1$ μM (Klee et al. 1980). As described in *Simulations of the experiment of Malenka et al. with standard dynamics,* we varied k_f and k_r in the range of 0.05 μM/ms $\leq k_f \leq$ 5 μM/ms and 0.05 ms$^{-1} \leq k_r \leq$ 5 ms^{-1}. We have chosen k_f = 0.5 μM/ms and k_r = 0.5 ms^{-1} as standard values.

There are two known calcium extrusion mechanisms, the CaATPase, an ATP-driven Ca^{2+} pump, and the Ca/Na exchange (Dipolo and Beaugé 1983). The first is a low-capacity, high-affinity pump, whereas the latter is a high-capacity, low-affinity mechanism. Little is known, however, about the density of these extrusion mechanisms in hippocampal neurons. Following Zador et al. (1990), we use first-order Michaelis-Menton kinetics to describe each of the two extrusion mechanisms, i.e.

$$\frac{\partial[Ca^{2+}]}{\partial t} = \frac{A}{V}\left\{J_{leak} - P_sK_{max}\frac{[Ca^{2+}]}{[Ca^{2+}] + K_d}\right\} \quad (9)$$

Here A is the surface area and V the volume of the compartment under consideration. The leak flux J_{leak} was adjusted such that at a resting concentration of 50 nM the net extrusion of calcium was zero (Table 2). The value of K_d was taken from Zador et al. (1990). Because reliable values of the pump surface density P_s and the maximum turnover rate K_{max} are not available to us, the product P_sK_{max} has been considered a free parameter. It has been adjusted such that a 50-Hz stimulation applied at N = 10 synapses leads to a maximum Ca^{2+} of ~1 μM as in the experiment of Muller and Connor (1991). Figure 5 shows that a pump efficiency of $P_sK_{max} = 1 \times 10^{-15}$ μmol/(ms · μm^2) for the ATPase and $P_sK_{max} = 5 \times 10^{-15}$ μmol/(ms · μm^2) for the Na/Ca exchange yields a satisfying result, whereas a lower pump efficiency leads to a unrealistically high Ca^{2+}. Note that Zador et al. (1990) use a value of the pump efficiency that is smaller by a factor of 10. Thus calcium extrusion is less efficient in their model. On the other hand, there is also less calcium influx into the spine head, because, in their model, the NMDA current contains a calcium fraction of 2% only. The two parameter changes roughly compensate each other and lead to about the same Ca^{2+} in the spine head. Our standard set of parameters has been summarized in Table 2. Figure 3*C* shows the typical time course of $[Ca^{2+}]$ generated by stimulation of 1 synapse (*inset*) or 30 synapses (full-sized graph).

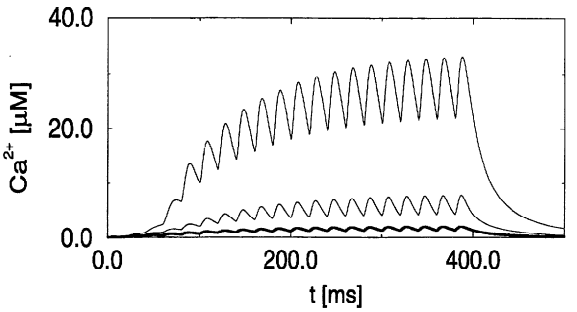

FIG. 5. Ca^{2+} concentration ($[Ca^{2+}]$) in the spine head after 20 impulses at 50 Hz. N = 10 synapses have been stimulated simultaneously ("weak stimulation" paradigm). With the standard set of parameters [buffering rates k_f = 0.5 (μM · ms)$^{-1}$, k_r = 0.5 ms^{-1}; pump efficiency $P_sK_{max} = 1 \cdot 10^{-15}$ μmol/(ms · μm^2) for ATPase and $5 \cdot 10^{-15}$ μmol/(ms · μm^2) for Na/Ca exchange)], the average calcium concentration is in the range of a few μM (thick line). If the pump efficiency is reduced by a factor of 2 (*middle trace*) or 5 (*top trace*), the calcium concentration is much higher.

TABLE 2. *Parameters of calcium dynamics*

Calcium dynamics		
Diameter, spine head	d_{head}	0.5 μm
Diameter, spine neck	d_{neck}	0.1 μm
Diffusion constant	D	0.6 μm^2/s
Initial concentration of calcium	$[Ca^{2+}]_i$	50 nM
Calcium fraction of NMDA current	I_{Ca}/I_{NMDA}	0.1
Concentration of buffering sites	$[bu_{tot}]$	120 μM
Forward buffering rate	k_j	0.5 μM/ms
Backward buffering rate	k_b	0.5 ms^{-1}
Calcium pumps		
Pump efficiency, ATPase	P_sK_{max}	1×10^{-15} μmol/(ms · μm^2)
Pump efficiency, Na/Ca exchange	P_sK_{max}	5×10^{-15} μmol/(ms · μm^2)
Pump affinity, ATPase	K_d	0.5 μM
Pump affinity, Na/Ca exchange	K_d	20 μM
Leakage flux, ATPase	J_{leak}	0.1×10^{-15} μmol/(ms · μm^2)
Leakage flux, Na/Ca exchange	J_{leak}	1.25×10^{-17} μmol/(ms · μm^2)
Calcium stores		
Total volume	V_{store}	0.1 × $V_{spinehead}$
Initial calcium concentration	$[Ca]_{store}$	25 mM
Depletion rate	ρ	(150 ms)$^{-1}$
Store time constant	τ_{store}	100 ms
Calcium response threshold	$[Ca^{2+}]_\theta$	150 μM
Calcium response maximum	$[Ca^{2+}]_{max}$	250 nM

For abbreviations, see Table 1.

Model of intracellular calcium stores

As mentioned in the INTRODUCTION, it is most likely that Ca^{2+} stores play an important role in the induction of LTP. We studied a model of intracellular stores in the spine head of a synapse, in particular the dynamics of calcium release by this store. Intracellular stores consist of three components: pumps to sequester calcium, calcium binding proteins such as calcineurin to store calcium, and RYR and $InsP_3$ receptor channels to release calcium from the stores. Neurons are supposed to contain both receptor types. For a detailed review see Berridge (1993).

To activate the $InsP_3$ receptor both $InsP_3$ and calcium are needed. The dependence on $InsP_3$ is a all-or-none response, viz., the receptor is inactive below some critical value and becomes active above it (Berridge 1993). The activation level depends on the calcium concentration of the surrounding medium. As the concentration of Ca^{2+} rises it becomes increasingly active. Beyond a Ca^{2+} of ~200–300 nM, $InsP_3$ becomes inhibitory (Bezprozvanny et al. 1991). Thus there is a bell-shaped calcium response (Bezprozvanny et al. 1991; Finch et al. 1991). The RYR receptor displays a similar bell-shaped calcium dependence (Hymel et al. 1988), but it seems that no coagonist is needed. Because there may be different subtypes of receptors with varying characteristics in different types of neurons and because little is known about these receptors in CA1 neurons, a model of their properties can only be qualitative. In particular, the mechanism of how the two types of receptors contribute to calcium release during LTP induction is still unclear. We therefore have decided to model both receptors by a single, phenomenological equation. This seems to be reasonable because both mediate calcium-induced calcium release with a similar bell-shaped calcium-dependent response.

Not much is known about the number and shape of intracellular calcium stores in CA1 neurons. For reasons of simplicity we as-

sumed that there is a single store in the spine head. Its volume was set to be 1/10 of the spine head volume. The store was placed in the second diffusion compartment; see Fig. 4. Because calcium released from the store spreads almost instantaneously all over the spine head, the shape and distribution of buffers is of no importance for our results. For the maximum concentration of stored Ca^{2+}, we have chosen values between 2 and 25 mM. These values are consistent with measurements in frog muscle sarcoplasmic reticulum (Hasselbach and Oetliker 1983).

In our model the dynamics of calcium release from the store is given by

$$\frac{\partial[Ca^{2+}]_{store}}{\partial t} = \rho X \{[Ca^{2+}]_{store} - [Ca^{2+}]_{spine}\} \quad (10)$$

where $[Ca^{2+}]_{store}$ and $[Ca^{2+}]_{spine}$ are the calcium concentrations inside the store and in the spine head, respectively. The depletion rate ρ depends on the number of channels, the maximum channel conductivity, and the volume of the store. In our simulations we use $\rho = 1/(150\ \text{ms})$. The factor X is the fraction of open channels, which depends on both the calcium concentration in the spine and the probability (RA) of receptor agonist binding. To be specific, we assume first-order kinetics, viz.

$$\frac{d}{dt}X = -\frac{1}{\tau_{store}}\{X - (RA)Re([Ca^{2+}]_{spine})\} \quad (11)$$

where $Re([Ca^{2+}]_{spine})$ models the bell-shaped Ca^{2+} response of the receptors and τ_{store} is some channel time constant. We have checked that our results are not sensitive to the value of τ_{store} and we have fixed τ_{store} to 100 ms. As mentioned before, (RA) is the probability of receptor agonist binding. In our simulations, we consider two situations, viz., first the case where no agonist is available, that is $(RA) = 0$, and second, the case where we have a large amount of agonist (e.g., $InsP_3$). In the latter situation all available receptor sites are saturated and we set (RA) at 1.

Equations 10 and *11* are assumed to give a phenomenological description of Ca^{2+} transport out of the store and are certainly not a full model of the microscopic processes of calcium release from the store. In all simulations the store contained a maximum amount of Ca^{2+} at the beginning of the simulated experiment. In our model, the calcium response $Re([Ca^{2+}])$ is 0 below a threshold value of $[Ca^{2+}]_\theta$ of 150 nM. For $[Ca^{2+}]_{spine} > [Ca^{2+}]_\theta$ it obeys the equation

$$Re([Ca^{2+}]_{spine}) = R_0 \frac{[Ca^{2+}]_{spine} - [Ca^{2+}]_\theta}{[Ca^{2+}]_{max} - [Ca^{2+}]_\theta} \exp\left[-\frac{[Ca^{2+}]_{spine} - [Ca^{2+}]_\theta}{[Ca^{2+}]_{max} - [Ca^{2+}]_\theta}\right] \quad (12)$$

a so called α-function; cf. Fig. 6. The response function $Re([Ca^{2+}])$ takes its maximum of 1 at a concentration of $[Ca^{2+}]_{max} = 250$ nM, which is in the range of measured values for

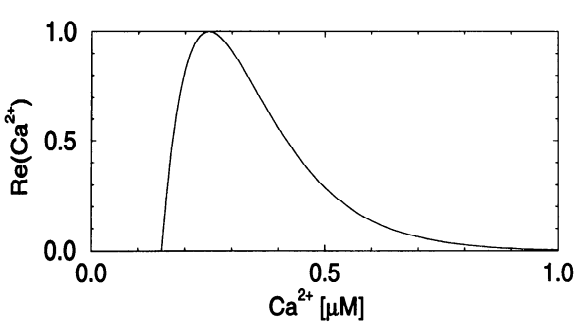

FIG. 6. Bell-shaped Ca^{2+} response $Re([Ca^{2+}])$ of the receptor as a function of the calcium concentration. The curve has its maximum at an intracellular $[Ca^{2+}]$ of 250 nM. The maximum is scaled to the value of 1. The response vanishes for $[Ca^{2+}] < 150$ nM.

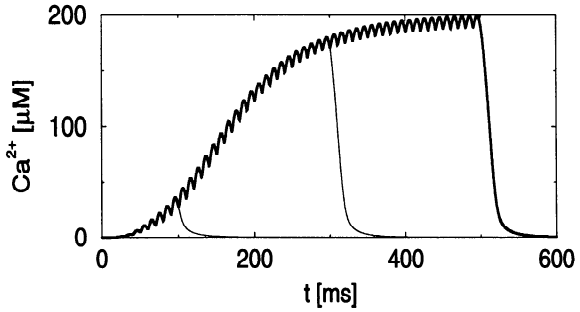

FIG. 7. Decay of intracellular $[Ca^{2+}]$ after 10 impulses, 30 impulses (thin lines), or 50 impulses (thick line) at 100 Hz. $N = 20$ synapses have been stimulated simultaneously (strong stimulation paradigm). In all cases the decay is fast and the resting concentration is reached within ~100 ms.

$InsP_3$ receptors (Bezprozvanny et al. 1991). The prefactor $R_0 = \exp(1)$ is a normalization constant. The exact functional form of the response function is somewhat arbitrary. We have chosen an α-function because it describes the steep rise in calcium-dependent receptor activation at nanomolar levels for both receptor types. At the same time, it allows for a slow decrease at higher concentrations, which takes into account that RYR receptors are deactivated only at higher calcium concentrations up to the micromolar level. (Bezprozvanny et al. 1991).

RESULTS

In the first part of this section we show that standard Ca^{2+} dynamics cannot account for the time course of Ca^{2+} during LTP induction, as found in experiments by Malenka et al. (1992). The second and third parts deal with the results obtained with the extended model including intracellular Ca^{2+} stores. It is shown that the extended model can in fact account for the 2-s criterion (*Simulations of the experiment of Malenka et al. with intracellular stores*). Finally, in *Intracellular stores with primed and theta-burst stimulation,* we apply the extended model to the primed and theta-burst stimulation paradigm.

Simulations of the experiment of Malenka et al. with standard dynamics

As a first step, we stimulated the model neuron with spike trains of 10–50 impulses at 100 Hz (Fig. 7). Independent of the number of impulses, the intracellular Ca^{2+} decays within 100–200 ms to its resting value after the end of the stimulation. The Ca^{2+} should, however, stay significantly above its resting value for ≥ 1 or 1.5 s after the end of the stimulation in order to account for the "2-s criterion."

In our simulations we varied all relevant parameters systematically in order to find a reasonable set of constants that would yield an increased calcium level for sufficiently long times. In a first attempt we varied the buffering constants k_f and k_r in a reasonable regime (i.e., by a factor of 1/10 or 10 and combinations thereof). The buffers serve as short-time integrators that smooth the time course of the intracellular Ca^{2+}. Buffering also has some influence on the peak value of calcium concentration during stimulation; cf. Holmes and Levy (1990), Gold and Bear (1994). A change of the buffering constants does not, however, prolong the calcium decay after stimulation.

Next we reduced the Ca^{2+} fraction of the NMDA current

to 2% (cf. Zador et al. 1990). As a result, the overall Ca^{2+} during stimulation is significantly lower. The decay time after stimulation remains unchanged.

Examining the effects of the Ca^{2+} extrusion mechanisms is a rather complicated and arduous task because there are many potentially relevant parameters. In some cases (with very weak pumps) even the influence of dendritic calcium comes into play. We conducted many simulations examining this problem and find that a decrease in pump efficiency has a similar effect to that of an increase of the Ca^{2+} fraction of the NMDA current. A typical result with reduced pump efficiency is shown in Fig. 5. If the pump efficiency is lowered by a factor of 5, the weak stimulation paradigm (50 Hz at $N = 10$ synapses) leads to an average Ca^{2+} of $\sim 20\ \mu M$ in the spine head. This value must be considered unrealistic because it is much larger than the one suggested by the experiments of Muller and Connor (1991). Note that, independent of the pump efficiency, the decay of the Ca^{2+} is rather fast and occurs within some 100 ms.

In conclusion, all of the above simulation results indicate that an additional active Ca^{2+} source that sustains an increased Ca^{2+} level after the end of a tetanic stimulation is necessary to explain the 2-s criterion. It is not possible to change the parameters of passive decay such that there is a clear elevation of intracellular Ca^{2+} levels lasting 1–2 s after the end of the stimulation. As will be shown in the next two parts, intracellular stores can take over the role of this source.

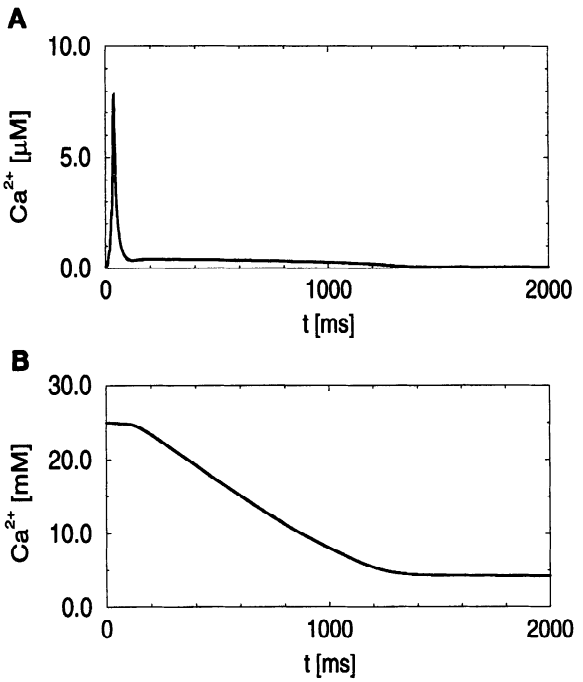

FIG. 8. *A*: time course of $[Ca^{2+}]$ in the spine head with the extended model including an internal store. Starting at $t = 0$, 4 impulses at 100 Hz have been applied at $N = 30$ synapses. *B*: decay of the $[Ca^{2+}]$ in the store during the above simulation. Calcium release from the store extends over >1 s. During this time an elevated calcium level is sustained in the spine head (*A*), while the calcium concentration in the store drops steadily (*B*).

Simulations of the experiment of Malenka et al. with intracellular stores

In this part we present results with the extended model including intracellular calcium stores. We simulated the scenario of Malenka et al. (1992), but because we are interested in the decay, we restricted the stimulation to four impulses at 100 Hz ($N = 30$). Figure 8*A* shows the time course of Ca^{2+} in a simulation where we used an initial calcium concentration of 25 mM for the store. It can be seen that Ca^{2+} levels >400 nM can be maintained for >1 s. Because of the bell-shaped response function, calcium release is not possible while the intracellular Ca^{2+} is high, as during stimulation. After the end of the stimulation at $t = 30$ ms, the internal calcium concentration drops rapidly. If the calcium concentration has decreased to ~500 nM, the stores open and additional calcium is released. We note that the exact duration of the period during which the Ca^{2+} is significantly above its resting value depends on parameters such as the size of the store, the initial Ca^{2+} inside the store, the dimensions of the spine, and the pump rates. Because the present model is supposed to be qualitative, we did not examine this dependence in more detail. There are, however, certain requirements concerning the minimum amount of stored calcium. In Fig. 8*B*, the time course of Ca^{2+} inside the store during the simulation of Fig. 8*A* is plotted. During the stimulation, the intracellular calcium concentration is high and blocks the release. Comparing Fig. 8, *A* and *B*, it is evident that the Ca^{2+} in the spine head stays at relatively high values (>400 nM) as long as the store is not empty and is able to supply extra calcium to compensate for the loss of calcium due to extrusion and diffusion. This accounts for the almost linear decline of the Ca^{2+} in the store. In this regime, the receptor activation function can be understood as a controller in a closed circuit. If the store is nearly empty, calcium release stops and standard Ca^{2+} decay takes over. The specific time dependence of the decay depends on the form of the activation function *Re*. We used an α-function because it is easy to compute and its maximum can be easily adjusted. It should be clear that there are more complicated activation functions that might contain additional parameters by which the decay can be modified in different ways. We feel, however, that our model with a bell-shaped α-function-type calcium response yields reasonable results.

Intracellular stores with primed and theta-burst stimulation

To demonstrate the power of the above concept of intracellular stores, we applied our model to a scenario of primed and theta-burst stimulation. Before we discuss the results of our simulations, we give a short overview of the specific properties of both paradigms.

A priming stimulus (e.g., 4 impulses at 100 Hz) followed by a burst of four impulses at 100 Hz at another group of synapses applied after an interburst interval of 200 ms is termed "primed burst stimulation." Experiments with variable interburst intervals were conducted by Larson and Lynch (1986). It turned out that strongest LTP was induced at an interburst interval of 200 ms. LTP was weak at an interval of 100 ms and invisible at an interval of 2,000 ms. For reasons of simplicity we refer to all of these stimulation patterns as the primed burst scenario.

In other experiments Larson and Lynch applied several

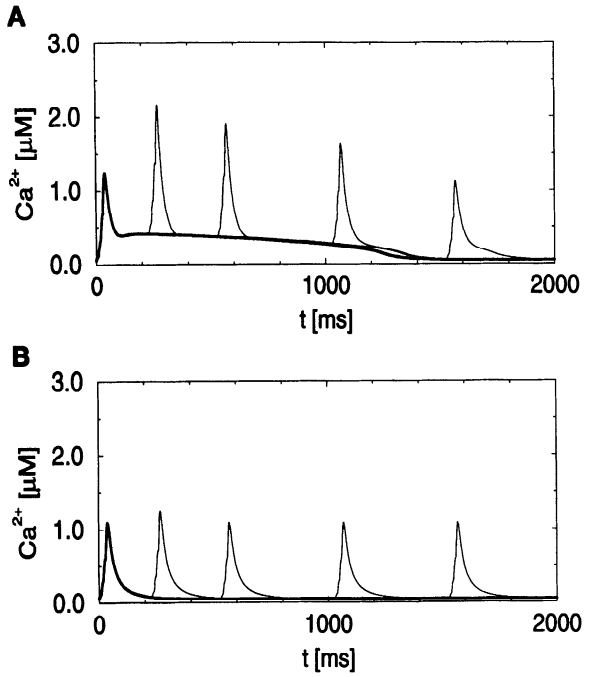

FIG. 9. Variation of interburst intervals. The calcium concentration in the spine head is plotted as a function of time. A 1st burst of 4 impulses at 100 Hz applied at $N = 10$ synapses starts at $t = 0$. Five different runs are superimposed in the same plot, i.e., the situation with no further burst (thick line) and with a 2nd burst after 200, 500, 1,000, or 1,500 ms (thin lines). *A*: in the extended model including intracellular stores, the calcium concentration remains at an approximately constant level for ~1,000 ms (thick line). With a 2nd burst after 200, 500, or 1,000 ms, the calcium concentration reaches a peak value that is significantly higher than during the 1st burst. *B*: in the standard model without stores, the 2nd peak is hardly affected by the 1st burst, except for the case of a short interburst interval.

bursts of four impulses at 100 Hz with variable interburst intervals to a single group of synapses (Larson et al. 1986). This stimulation pattern is termed "theta-burst stimulation." The strength of the induced LTP has a similar dependence on the interburst interval to the one found with the primed burst scenario. The strongest LTP is induced at an interval of 200 ms; intervals of 100 and 1,000 ms induce weaker LTP; but virtually no LTP has been found with intervals of 2,000 ms. Below we refer to these experiments as the theta-burst scenario. The similarities in the induction of LTP indicate, in our opinion, that both scenarios are based on the same microscopic effects. We have therefore simulated a single scenario that is supposed to cover qualitatively both primed and theta-burst experiments. As our stimulation paradigm, we take two bursts with four impulses at 100 Hz each ($N = 10$) and vary the interburst interval. We thus take a property of the primed burst scenario, two stimuli only, and combine it with a property of the theta-burst scenario, namely stimulating a single group of synapses. A discussion of the limitations of this approach will be deferred to the DISCUSSION section.

Figure 9*A* shows the results of a simulation of the above scenario. Several runs with variable interburst intervals are plotted in the same graph. The first peak of the intracellular Ca^{2+} is due to influx of extracellular calcium during the first burst. After the burst, the stores open and the Ca^{2+} stays at an elevated level (thick line). If a second burst is applied after an interburst interval of 200, 500, 1,000, or 1,500 ms (thin lines), the Ca^{2+} shows a second peak. The peak amplitude is maximal for an interburst interval of 200 ms. It is slightly reduced but still larger than in the model without stores (Fig. 9*B*) for interburst intervals of 500 or 1,000 ms. The store has, however, no effect if the interburst interval is $\geq$1,500 ms.

These results regarding the time course of the calcium concentration can be related to LTP induction if one assumes that LTP is possible only if the peak Ca^{2+} exceeds a critical concentration Ca_c^{2+}. In a simple model, we can take the strength of LTP to be proportional to the excess concentration $Ca^{2+} - Ca_c^{2+}$. If the critical concentration necessary for LTP induction is ~1.5 μM, then according to our simulation results of Fig. 9*A*, LTP can be induced at interburst intervals of 200, 500, or 1,000 ms, but not with an interburst interval of 1,500 ms.

DISCUSSION

This section is divided into two parts. In the first part we discuss conclusions from our simulations of the experiment of Malenka et al. (1992) concerning the possible role of intracellular Ca^{2+} stores in the induction of LTP. In the second part we focus on the interpretation of the results relating to the primed and theta-burst stimulation paradigm.

The experiments of Malenka et al. (1992) indicate an elevation of the intracellular Ca^{2+} during 1–1.5 s after the end of the stimulus for this particular stimulation pattern. We do not know whether this would also hold for other experimental paradigms of LTP induction. In any case, the experiments of Malenka et al. can be used to check the plausibility of some models of calcium dynamics. As shown in *Simulations of the experiment of Malenka et al. with standard dynamics,* standard calcium dynamics fails to give a time course of Ca^{2+} in the spine head, consistent with the experiments of Malenka et al. (1992). NMDA channels close rapidly after the end of the stimulation and cannot sustain a persistent rise in intracellular calcium. Furthermore, the standard model cannot be adapted by a mere change of parameters. Thus an additional source of calcium is needed. As mentioned in INTRODUCTION, there is growing evidence for an important contribution of RYR-and $InsP_3$-receptor-mediated calcium release from intracellular stores. We have introduced a model of intracellular stores with bell-shaped calcium response and have shown that calcium-induced calcium release from stores can indeed account for a significant elevation of the intracellular calcium level after the end of synaptic stimulation. Of course, such a model cannot be quantitative because the distribution of intracellular stores and the properties of receptors in CA1 pyramidal cells are not known in sufficient detail. Our studies suggest, however, that the bell-shaped Ca^{2+} response, a common property of both RYR and $InsP_3$ receptors, plays an important role. In fact, with a bell-shaped response, calcium release from the store starts only after the stimulation when the Ca^{2+} drops below a certain value.

We emphasize that our model is not intended to give a detailed description of the molecular processes leading to calcium release from the stores. In particular, we do not

model the reaction chain leading to a binding of the agonist (e.g., $InsP_3$) to the receptor; cf. *Eq. 11*. In the present version of our model we simply assume that a sufficient amount of $InsP_3$ (or none at all) is available at the stores. In this case, a short burst of three or four spikes arriving at a single synapse will trigger the process of calcium release from the stores. Furthermore, if the pump efficiency $P_s K_{max}$ is reduced (cf. Zador et al. 1990), then even a single spike at a single synapse starts the process of calcium release, a result that is rather implausible. The fact that the calcium release can be triggered even by a small amount of calcium is generic and not sensitive to buffer rates and neuronal time constants. On the other hand, the process of self-sustained calcium release is sensitive to the depletion rate ρ and the portion of open channels X. If ρ or X is reduced by a factor of 10, calcium supply from the stores is not sufficient to compensate the loss due to diffusion and extrusion. In this case a sustained calcium release cannot be achieved, not even after a strong stimulation of the neuron. Thus our model of intracellular stores shows two completely different regimes. For low values of ρ and X, self-sustained calcium release is not possible at all; for higher values, calcium release from the stores is induced even by a small number of spikes. The amount of agonist (e.g., $InsP_3$) could be used to switch between the two regimes. This suggests an important role of metabotropic glutamate receptors, because $InsP_3$ can be produced by a reaction chain starting at metabotropic glutamate receptors (Bliss and Collingridge 1993). In the present version of the model, the mechanisms of $InsP_3$ production are not described explicitly, but we suppose that our main results remain unchanged, if the dynamics of metabotropic glutamate receptors and $InsP_3$ are included.

We mention that stores are not the only solution that yields a sustained increase in Ca^{2+}. Alternatively, voltage-dependent Ca^{2+} channels could serve as long-lasting calcium sources. Calcium channels are known to play an important role during LTP induction in CA3 mossy fiber synapses (Fisher and Johnston 1990; Jaffe and Johnston 1990) and in kitten visual cortex (Komatsu and Iwakiri 1992). To account for the 2-s criterion, such channels must have intrinsic time constants longer than a few hundred milliseconds. Otherwise they close as soon as the membrane potential returns to the resting value, i.e., within 100–200 ms; cf. Fig. 3. In the present study we have neglected the potential relevance of voltage-dependent calcium channels and have focused on intracellular stores in spines of hippocampal CA1 neurons.

There is overwhelming experimental evidence that NMDA receptors are crucial for LTP induction in CA1 neurons (Bliss et al. 1993), but, as we have shown here, they cannot be the only Ca^{2+} source. Both our results and the experiments of Malenka et al. (1992) suggest that there might be two basic effects due to the intracellular Ca^{2+} playing an important role in the induction of LTP.

1) Brief tetanic stimulation or other special stimulation patterns cause short but high peaks in the intracellular Ca^{2+} because of calcium influx through NMDA channels, which might trigger a biochemical reaction chain.

2) To maintain the reaction chain and eventually induce LTP, a persistent rise in the intracellular Ca^{2+}, possibly at lower levels around a few hundred nanomolars, is necessary. This is the potential task of intracellular stores.

The way in which both effects interact could determine the duration and strength of the induced potentiation. We are aware of the fact that because of uncertainties in the measurement of important parameters such as pump efficiency, buffer rate, channel conductivity, or the distribution of intracellular stores, the model as well as our conclusions cannot be quantitative. But, in our opinion, stores lead to an interesting and potentially relevant behavior that deserves examination by future experiments.

As we have shown in the previous section, our theory of intracellular stores can also explain some of the temporal requirements of primed and theta-burst stimulation. With primed or theta-burst stimulation, LTP can be induced if the interburst interval is in the range of 200–1000 ms. This suggests that two different time constants indicating two different processes are involved. We make no attempt to explain the molecular process leading to the minimum interburst interval of 200 ms. This time constant could be due to the reaction chain starting at metabotropic glutamate receptors, which eventually leads to binding of $InsP_3$ at the stores, a sequence of reactions that is not modeled in our present work. Our model of intracellular stores does, however, provide a plausible scenario for the 1,000-ms time constant. Because of their similar dependence on interstimulus intervals, we have assumed that the same processes are involved both in primed and theta-burst stimulation. This means that theta-burst stimulation is equivalent to a repeated primed burst stimulation. Larson and Lynch (1986) have demonstrated that the first burst causes a diffuse priming effect all over the neuron that lasts for ~2 s. Because of this, long-duration depolarization alone cannot be the main cause of priming. We suggest that the priming burst induces an influx of calcium through voltage-gated calcium channels at each spine. The influx alone would not be sufficient to induce LTP, but it causes intracellular stores to release calcium, if the agonist $InsP_3$ or RYR is available. As we have seen in the last section, the release has a characteristic time of 1–2 s. This allows us to suggest the following interpretation. The first burst does not induce LTP, because the critical level of Ca^{2+} is not reached, but it triggers calcium release from the stores. When the second burst is applied, the influx of Ca^{2+} through NMDA channels at the stimulated synapses and the remaining efflux of Ca^{2+} from intracellular stores sum up to a peak Ca^{2+} high enough to induce LTP. Because of buffer saturation this summation is nonlinear, which means that relatively high concentrations can be reached with a rather weak stimulation pattern. The induction of LTP with theta-bursts could work in the same way. The only difference is that "priming" is applied at the same synapses as the following burst.

To summarize, we have presented a model of intracellular Ca^{2+} stores that can explain several experimental results, in particular the primed and theta-burst scenario, which cannot be explained by standard calcium dynamics. Because of a lack of experimental data, however, our model must remain tentative. Future experiments will hopefully supply enough data for refining the model to allow fully quantitative predictions.

Address reprint requests to W. Gerstner.

Received 11 July 1994; accepted in final form 13 April 1995.

REFERENCES

AMIT, D. J. *Modeling Brain Function.* Cambridge, UK: Cambridge Univ. Press, 1989.

BERRIDGE, M. J. Inositol trisphosphate and calcium signaling. *Nature Lond.* 361: 315–325, 1993.

BEZPROZVANNY, I., WATRAS J., AND EHRLICH, B. E. Bell-shaped calcium-response curves of Ins(1,4,5)P3-gated and calcium-gated channels from endoplasmatic reticulum of cerebellum. *Nature Lond.* 351: 751–754, 1991.

BINDMAN, L., CHRISTOFI, G., MURPHY, K., AND NOWICKY, A. Long-term potentiation (ltp) and depression (ltd) in the neocortex and hippocampus: an overview. In: *Aspects of Synaptic Transmission,* edited by T. W. Stone. London: Taylor & Francis, 1991, vol. 1, p. 3–25.

BLISS, T. V. P. AND COLLINGRIDGE, G. L. A synaptic model of memory: long-term potentiation in the hippocampus. *Nature Lond.* 361: 32–39, 1993.

BORTOLOTTO, Z. A. AND COLLINGRIDGE, G. L. Characterization of LTP induced by the activation of glutamate metabotropic receptors in area CA1 of the hippocampus. *Neuropharmacology* 32: 1–9, 1993.

BROWN, T. H., CHANG, V. C., GANONG, A. H., KEENAN, C. L., AND KELSO, S. R. Biophysical properties of dendrites and spines that may control the induction and expression of long-term synaptic potentiation, In: *Long-Term Potentiation: From Biophysics to Behavior,* edited by P. W. Landfield and S. Deadwyler. New York: Liss, 1988, p. 201–264.

BROWN, T. H., FRICKE, R. A., AND PERKEL, D. H. Passive electrical constants in three classes of hippocampal neurons. *J. Neurophysiol.* 46: 812–827, 1981.

BROWN, T. H., ZADOR, A. M., MAINEN, Z. F., AND CLAIRBORNE, B. J. Hebbian modifications in hippocampal neurons. In: *Long-Term Potentiation,* edited by M. Baudry and J. L. Davis. Cambridge, MA: MIT Press, 1991, p. 357–389.

CARAFOLI, E. Intracellular calcium homeostasis. *Annu. Rev. Biochem.* 56: 395–433, 1987.

DIPOLO, R. AND BEAUGÉ, L. The calcium pump and sodium-calcium exchange in squid axons. *Annu. Rev. Physiol.* 45: 313–324, 1983.

DOMANY, E., VAN HEMMEN, J. L., AND SCHULTEN, K. (Editors). *Models of Neural Networks.* Berlin: Springer-Verlag, 1991.

FINCH, E. A., TURNER, T. J., AND GOLDIN, S. M. Calcium as a coagonist of inositol 1,4,5-trisphosphate induced calcium release. *Science Wash. DC* 252: 443–446, 1991.

FISHER, R. AND JOHNSTON, D. Differential modulation of single voltage-gated calcium channels by cholinergic and adrenergic agonists in adult hippocampal neurons. *J. Neurophysiol.* 64: 1291–1302, 1990.

GAMBLE, E. AND KOCH, C. The dynamics of free calcium in dendritic spines in response to repetitive synaptic input. *Science Wash. DC* 236: 1311–1315, 1987.

GARASCHUK, O., SCHNEGGENBURGER, R., SCHIRRA, C. TEMPIA, F., AND KONNERTH, A. Fractional calcium currents through glutamate receptor channels in hippocampal CA1 pyramidal neurons. In: *Learning and Memory, Proceedings of the 23rd Göttingen Neurobiology Conference 1995,* edited by N. Elsner and R. Menzel. Stuttgart, Germany: Georg Thieme Verlag 1995, vol. 1, p. 112.

GASIC, G. P. AND HOLLMANN, M. A. Molecular neurobiology of glutamate receptors. *Annu. Rev. Physiol.* 54: 507–536, 1992.

GOLD, J. I. AND BEAR, M. F. A model of dendritic spine Ca^{2+} concentration exploring possible basis for sliding synaptic modification threshold. *Proc. Natl. Acad. Sci. USA* 91: 3941–3945, 1994.

HARVEY, J. AND COLLINGRIDGE, G. L. Thapsigargin blocks the induction of long-term potentiation in rat hippocampal slices. *Neurosci. Lett.* 139: 197–200, 1992.

HASSELBACH, W. AND OETLIKER, H. Energetics and electrogenicity of the sarcoplasmic reticulum calcium pump. *Annu. Rev. Physiol.* 45: 325–339, 1983.

HEBB, D. O. *The Organization of Behavior.* New York: Wiley, 1949.

HERTZ, J., KROGH, A., AND PALMER, R. G. *Introduction to the Theory of Neural Computation.* Redwood City, CA: Addison-Wesley, 1991.

HINDMARSH, A. C. Odepack, a systematized collection of ode solvers. In: *Scientific Computing,* edited by R. S. Stepleman, M. Couves, R. Peskin, W. F. Ames, and R. Vichnevetsky. Amsterdam: North-Holland, 1983, p. 55–64.

HOLMES, W. R. AND LEVY, W. B. Insights into associative long-term potentiation from computational models of NMDA receptor-mediated calcium influx and intracellular calcium concentration changes. *J. Neurophysiol.* 63: 1148–1168, 1990.

HYMEL, L., MAKOTO, I., FLEISCHER, S., AND SCHINDLER, H. Purified ryanodine receptor of skeletal muscle sarcoplasmic reticulum forms Ca^{2+}-activated oligomeric Ca^{2+}-channels in planar bilayers. *Proc. Natl. Acad. Sci. USA* 85: 441–445, 1988.

JAFFE, D. AND JOHNSTON, D. Induction of long-term potentiation at hippocampal mossy fiber synapses follows a Hebbian rule. *J. Neurophysiol.* 64: 948–960, 1990.

KAY, A. R. Inactivation kinetics of calcium current of acutely dissociated CA1 pyramidal cells of the mature guinea-pig hippocampus. *J. Physiol. Lond.* 437: 27–48, 1991.

KITAJIMA, T. AND HARA, K. A model of the mechanisms of long-term potentiation in the hippocampus. *Biol. Cybern.* 64: 33–39, 1990.

KLEE, C. B., CROUCH, T. H., AND RICHMAN, P. G. Calmodulin. *Annu. Rev. Biochem.* 49: 489–515, 1980.

KOMATSU, Y. AND IWAKIRI, M. Low-threshold Ca^{2+} channels mediate induction of long-term potentiation in kitten visual cortex. *J. Neurophysiol.* 67: 401–410, 1992.

LARSON, J. AND LYNCH, G. Induction of synaptic potentiation in hippocampus by patterned stimulation involves two events. *Science Wash. DC* 232: 985–988, 1986.

LARSON, J., WONG, D., AND LYNCH, G. Patterned stimulation at the theta frequency is optimal for the induction of hippocampal long-term potentiation. *Brain Res.* 368: 347–350, 1986.

LISMAN, J. E. AND HARRIS, K. M. Quantal analysis and synaptic anatomy—integrating two views of hippocampal plasticity. *Trends Neurosci.* 16: 141–147, 1993.

MADISON, D. V., MALENKA, R. C., AND NICOLL, R. A. Mechanisms underlying long-term potentiation of synaptic transmission. *Annu. Rev. Neurosci.* 14: 379–397, 1991.

MALENKA, R. C., LANCASTER, B., AND ZUCKER, R. S. Temporal limits on the rise in postsynaptic calcium required for the induction of long-term potentiation. *Neuron* 9: 121–128, 1992.

MCNAUGHTON, B. L., BARNES, C. A., AND ANDERSEN, P. Synaptic efficacy and EPSP summation in granule cells of rat fascia dentata studied in vitro. *J. Neurophysiol.* 46: 952–966, 1981.

MÜLLER, B. AND REINHARD, J. *Neural Networks: An Introduction.* Berlin: Springer-Verlag, 1991.

MULLER, W. AND CONNOR, A. J. Dendritic spines as individual neuronal compartments for synaptic Ca^{2+} responses. *Nature Lond.* 354: 73–76, 1991.

OBENAUS, A., MODY, I., AND BAIMBRIDGE, K. G. Dantrolene-Na (dantrium) blocks induction of long-term potentiation in hippocampal slices. *Neurosci. Lett.* 98: 172–178, 1989.

PERETTO, P. An introduction to the modeling of neural networks. Cambridge, UK: Cambridge Univ. Press, 1992.

PERKEL, D. H. AND MULLONEY, B. Electrotonic properties of neurons: steady-state compartmental model. *J. Neurophysiol.* 41: 621–639, 1978.

PETZOLD, L. R. Automatic selection of methods for solving stiff and nonstiff systems of ordinary differential equations. *Siam J. Sci. Stat. Comput.* 4: 136–148, 1983.

TURNER, D. A. AND SCHWARTZKROIN, P. A. Steady-state electrotonic analysis of intracellularly stained hippocampal neurons. *J. Neurophysiol.* 44: 184–199, 1980.

SPRUSTON, N. AND JOHNSTON, D. Perforated patch clamp analysis of the passive membrane properties of three classes of hippocampal neurons. *J. Neurophysiol.* 67: 508–529, 1992.

ZADOR, A., KOCH, C., AND BROWN, T. H. Biophysical model of a Hebbian synapse. *Proc. Natl. Acad. Sci. USA* 87: 6718–6722, 1990.